14th Spacecraft Charging Technology Conference, ESA/ESTEC, Noordwijk, NL, 04-08 APRIL 2016

Deep Charging Evaluation of Satellite Power and Communication System Components

T. A. Schneider[1], J. A. Vaughn[1], B. Chu, F. Wong[2], G. Gardiner[2], K. H. Wright[3], and B. Phillips[4]

(1) NASA Marshall Space Flight Center, EM50, Huntsville, Alabama, USA
(2) Space Systems/Loral, LLC, Palo Alto, California, USA
(3) University of Alabama-Huntsville, Huntsville, Alabama, USA
(4) Aerodyne Incorporated, Huntsville, Alabama, USA

ABSTRACT

A set of deep charging tests has been carried out by NASA's Marshall Space Flight Center on subscale flight-like samples developed by Space Systems/Loral, LLC. The samples, which included solar array wire coupons, a photovoltaic cell coupon, and a coaxial microwave transmission cable, were placed in passive and active (powered) circuit configurations and exposed to electron radiation. The energy of the electron radiation was chosen to deeply penetrate insulating (dielectric) materials on each sample. Each circuit configuration was monitored to determine if potentially damaging electrostatic discharge events (arcs) were developed on the coupon as a result of deep charging. The motivation for the test, along with charging levels, experimental setup, sample details, and results will be discussed.

1. INTRODUCTION

Electric Orbit Raising (EOR) is an attractive option for communication satellite operators, as it provides a means to deploy satellites to Geostationary Earth Orbit (GEO) with reduced launch costs and increased payload mass [1]-[3]. Unfortunately, EOR does require spiraling through Earth's radiation belts, which exposes the satellite to high energy electron radiation [4], [5]. For spacecraft systems employing insulating materials, deep charging (or internal charging) can occur when they are exposed to a high energy electron environment [6]-[8].

Deep charging, in contrast to surface charging, focuses on electron penetration deep into insulating (dielectric) materials applied over conductors. A classic example of this scenario is an insulated wire. Deep charging can pose a threat to material integrity, and to sensitive electronics, when it gives rise to an electrostatic discharge or arc [9]-[11]. Fig. 1 is an illustration of a deep charging scenario, in which charges are accumulated in a layer inside an insulating material. The occurrence of an Electrostatic Discharge (ESD) event happens when the electric field formed by the deep charging electrons (and nearby grounded conductor) exceeds the breakdown strength of the dielectric material.

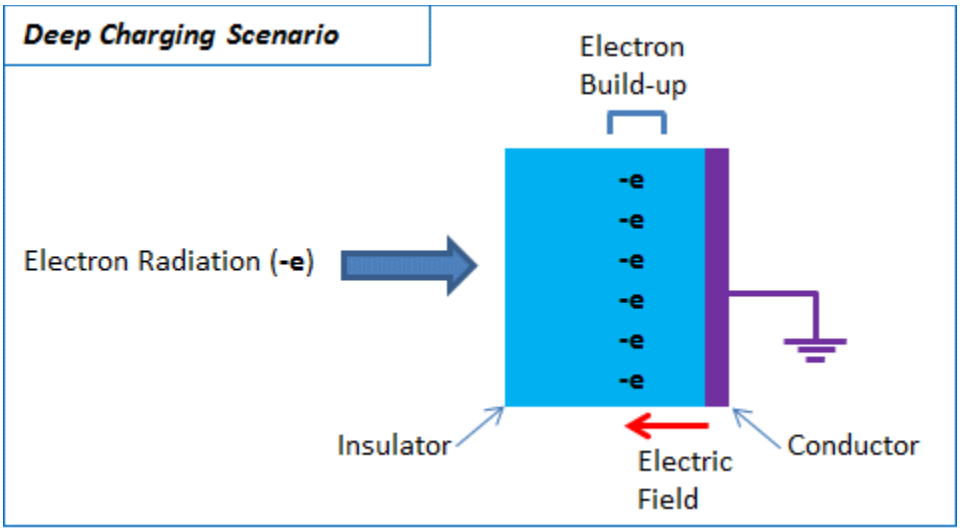

Figure 1. Illustration of the basic concept of deep (internal) charging

Models that predict deep charging scenarios do exist, and are being improved with added geometric effects (3D) and material properties [12]-[14]. These models are useful for gauging the likelihood of a deep charging ESD event, as they can determine if a predicted electric field formed from deep charging is close to known material breakdown limits. However, the precision of the models is ultimately limited when factors must be included such as imperfections and non-uniformity in materials, due to manufacturing or workmanship. Similarly, limited data on resistivity (in vacuum) of a new material, for example, can dramatically impact the precision of the model predictions.

A typical solar array system on a spacecraft includes multiple materials and layers with complicated geometries and subtle variations due to workmanship. Accurately modeling such a system is expensive and is ultimately limited by worst-on-worst case assumptions. Performing a deep charging test of the system, on the other hand, dramatically increases confidence in the spacecraft operator about the susceptibility (or immunity) of their real-world systems with respect to ESD events.

Space Systems Loral (SSL) has been using electric propulsion systems on their spacecraft for many years, and a natural extension of their experience with electric thrusters is Electric Orbit Raising (EOR). Recognizing that EOR requires multiple transits through Earth's radiation belts, SSL realized the potential for deep charging to occur on some of their systems – particularly systems directly exposed to the charging environment. Accordingly, SSL evaluated the radiation environment to determine electron flux and fluence levels and applied modeling to estimate deep charging in some materials [15].

To address deep charging concerns in complex spacecraft systems, SSL contracted with NASA's Marshall Space Flight Center to conduct experimental investigations into deep charging of subscale flight-like coupons. Details of the coupons selected, test setup challenges, and test results are discussed in this paper.

2. TEST ARTICLES

Exterior surfaces of spacecraft are, of course, directly exposed to the high energy charged particle environment and consequently can experience deep charging. For a communications satellite, two key

external systems are: 1) the solar array system; and 2) the microwave transmission system. Accordingly, SSL created test articles for the experimental investigation, which focused on these two systems. Each test article utilizes the same materials and components used in SSL's spacecraft manufacturing operations, however they have been scaled down to fit inside the vacuum test chambers.

2.1 Solar Array Power System Test Articles

Figs. 2 – 5 show the solar array power system test articles. A functioning solar array system requires photovoltaic cells, substrates, wiring, and connectors. The test articles provided by SSL comprise a complete solar array system – including front side (sun facing) and back side (rear surface) coupons. Each test article is a high fidelity test coupon which is flight-like in layout and functionality. The coupon with photovoltaic cells also incorporates interconnects and coverglass, and is known as a CIC (cell-interconnect-coverglass) coupon.

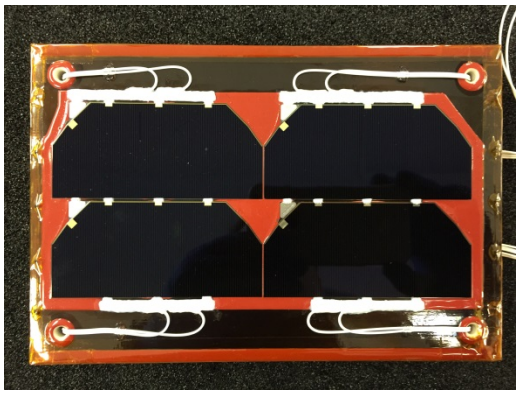

Figure 2. Cell-Interconnect-Coverglass (CIC) coupon. The coupon is composed of 2 strings. Each string is formed by connecting 2 cells in series.

Figure 3. Front Side Wire Coupon. The coupon represents wiring used to connect sections of the solar array together. Wire pairs are typically configured with a power system positive lead next to a return (or ground) lead.

Figure 4. Back Side Wire Coupon. This coupon represents the wiring on the back side of a solar array. The backside of the solar array employs a conductive Kapton material (which is black in color). Like the front side coupon, pairs of wires can represent the positive and return wires associated with the power system.

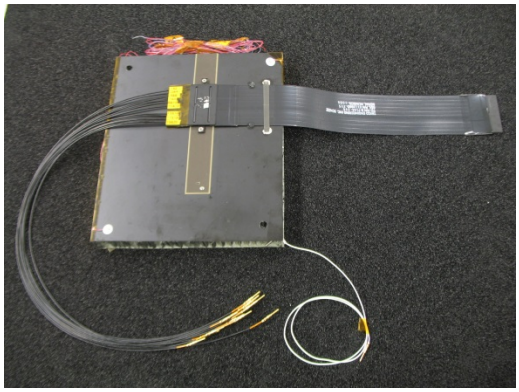

Figure 5. Ribbon Harness Coupon. It incorporates a flat connector that transitions from ribbon cables to round-wire cables. The coupon is mostly covered in conductive Kapton (black Kapton).

2.2 Microwave Communication Component

A key element of any spacecraft microwave communication system is the coaxial cables that carry the microwave signals between components in the receiving and transmitting sections of the assembly. An ESD event inside a coaxial cable can, at a minimum, create a signal disruption, or for extreme cases, destroy a small signal amplifier by injecting current directly into the component. Therefore, SSL selected a semi-rigid coaxial cable, often used for connecting external antennas, as a test article for the experimental investigation. Fig. 6 is a picture of the coaxial cable sample used in the deep charging test.

Figure 6. Coaxial cable sample. The cable is a semi-rigid cable with an Aluminum outer jacket. Each end of the cable is terminated with SMA male connectors. The sample was formed into a spiral geometry to maximize the area of the cable exposed to the electron beam.

3. TEST CONDITIONS

Conducting an experimental investigation helps reduce uncertainty associated with modeling results, since high fidelity test articles can be examined during actual electron beam exposures. Unfortunately, schedule and budget constraints prohibit investigating the full spectrum of energies and flux ranges spacecraft encounter while transiting the radiation belts. To optimize test time, SSL first examined electron fluxes and fluences in the radiation belts associated with EOR trajectories [15]. Next, SSL surveyed the test articles chosen and found areas that stood the greatest chance of experiencing deep charging. For the wire coupons, electrons with energy sufficient to penetrate into (but not beyond) insulation around the wires was of greatest interest. For the CIC coupon, electron accumulation in the coverglass on top of the photovoltaic cells, as well as under the cells in the Kapton substrate layer, posed the greatest risk for creating an ESD event which could directly affect the power system. Finally, for the semi-rigid coaxial cable, electrons with energy sufficient reach the Teflon jacket around the inner conductor were important to investigate.

Fig. 7 is an example of the modeling conducted by SSL to determine electron range in key areas of the test sample. The modeling shows 1 MeV electrons possess sufficient energy to penetrate the outer Aluminum jacket with a large population being deposited in the Teflon dielectric material (surrounding the inner conductor).

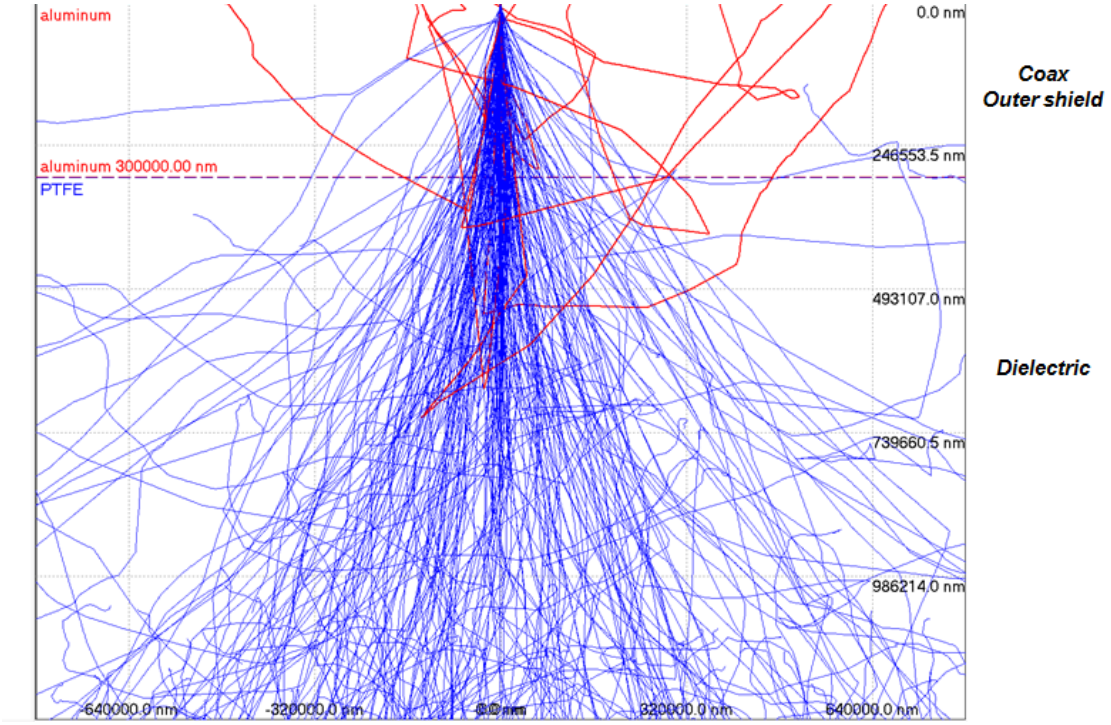

Figure 7. Simulation of 1MeV electron paths and range in a semi-rigid coaxial cable. The 1 MeV electron range in the coaxial cable shows charge deposition in the dielectric material surrounding the inner conductor.

SSL surveyed several electron energies to determine what energy posed a threat to produce deep (or internal) charging of the dielectrics on the various power system and communication system test articles. In the end, they found two electron energies could be chosen which provided deep charging of the dielectrics across the many different coupon configurations. Specifically, SSL chose 1 MeV and 300 keV for the electron energies to be used in the experimental investigation of their flight-like samples.

Having selected the electron energies of interest, SSL examined the fluxes and fluences associated with those energies for EOR transits in the radiation belts. Tables 1 and 2 show the test levels established by SSL.

Table 1. Electron Exposure Test Levels for CIC Coupon and Coaxial Cable Sample

Coupon Description	Fluence at 300 keV (e-/cm^2)	Fluence at 1 MeV (e-/cm^2)	Electron Flux (nA/cm^2)	Exposure Time at 300 keV (hrs)	Exposure Time at 1 MeV (hrs)
CIC Coupon	3.56E12	8.4E11	0.03	5.3	1.25
Coaxial Cable	3.56E12	8.4E11	0.03	5.3	1.25

Table 2. Electron Exposure Test Levels for Wire Coupons

Coupon Description	Fluence at 300 keV (e-/cm^2)	Fluence at 1 MeV (e-/cm^2)	Electron Flux (nA/cm^2)	Exposure Time at 300 keV (hrs)
Wire Coupon (front side)	3.56E12	N/A	0.03	5.3

Wire Coupon (back side)	3.56E12	N/A	0.03	5.3
Ribbon Coupon	3.56E12	N/A	0.03	5.3

4. TEST SETUP

4.1 Electron Beam Source

All of the testing was conducted using the Combined Environmental Effects Facility at NASA's Marshall Space Flight Center. The facility is anchored by two NEC Pelletron accelerators capable of delivering 760 keV protons and 2.5 MeV electrons. Both accelerator beam lines terminate in a cylindrical vacuum vessel where the sample under investigation is mounted. The sample chamber dimensions are 0.76 meter diameter and 1.5 meter length. For the deep charging investigation, only the electron accelerator was used. The electron beam is passed through a scattering foil as it enters the target chamber. At the target plane, the electron beam covers a 40 cm diameter circular area with 90% uniformity.

4.2 The Quest for an "ESD Clean" Chamber

The sample vacuum chamber was specially prepared for the deep charging investigation. Particular attention was focused on minimizing spurious ESD arcs on feed-through wiring, mounting hardware, and beam diagnostics. Fig. 8 is a picture of the back of the sample holder showing the wiring feeding into Aluminum tubes on the left side of the image. The Aluminum tubes were constructed of thick material designed to shield wiring from direct impingement of the high energy electrons as the wires connected the sample to the vacuum feed-through(s) inside a chamber port. Approximately 12cm of both the sample and chamber wiring was exposed in order to provide a means for connecting the sample to external circuitry. All such wiring was intentionally located immediately behind the sample and mounting hardware, which helped to reduce primary electron beam impingement on those areas. Given the large diameter of the electron beam, scattered electrons inside the vacuum chamber were a concern. To minimize surface charging due to low energy scattered electrons, Aluminum foil was placed around all exposed wiring and connections behind the sample.

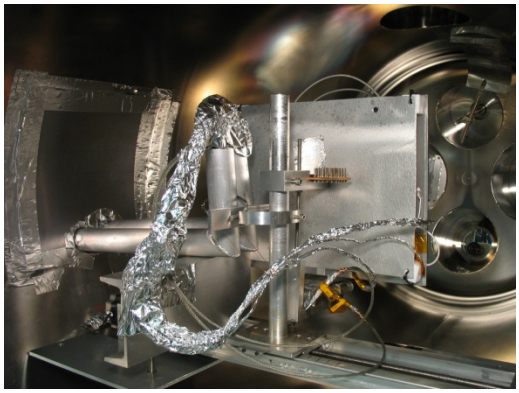

Figure 8. Picture of the area behind the sample mounting plate. Wires in the direct path of the electron beam are shielded in thick Aluminum tubes. Exposed sections of wire used to connect the sample to the external circuitry are placed behind the sample mounting plate to shield them from the electron beam. To reduce surface charging the wires are covered in Aluminum foil.

4.3 Detection Circuitry

The principal means of detecting an ESD event is measuring current pulses in wires attached to the sample under investigation. Typically, when dielectric breakdown occurs due to deep charging, there is a rapid flow of electrons from the arc site to ground – which manifests itself in the form of a pulse of current. Fig. 9 shows a basic block diagram of the ESD detection circuitry. The key diagnostic is inductive current probes which respond only to a change in current, i.e. current pulse. To increase the sensitivity of the current probes, the signal wire was wrapped several times through the core of the probe. A drawback to using multiple turns through a current probe is that the response time of the probe is reduced. Fig. 10 shows the results of a calibration test of the current probes. A square-wave current pulse is output from a device known as a "pulser" and connected through the current probes used in the investigation. In the case of a 5 microsecond long pulse, the current probe response closely follows the pulser signal. However the fidelity of the current probe response is reduced when trying to measure a 500 nano-second pulse. It is worth noting, however, the signal from the pulser is less than ideal at the 500 nano-second time scale.

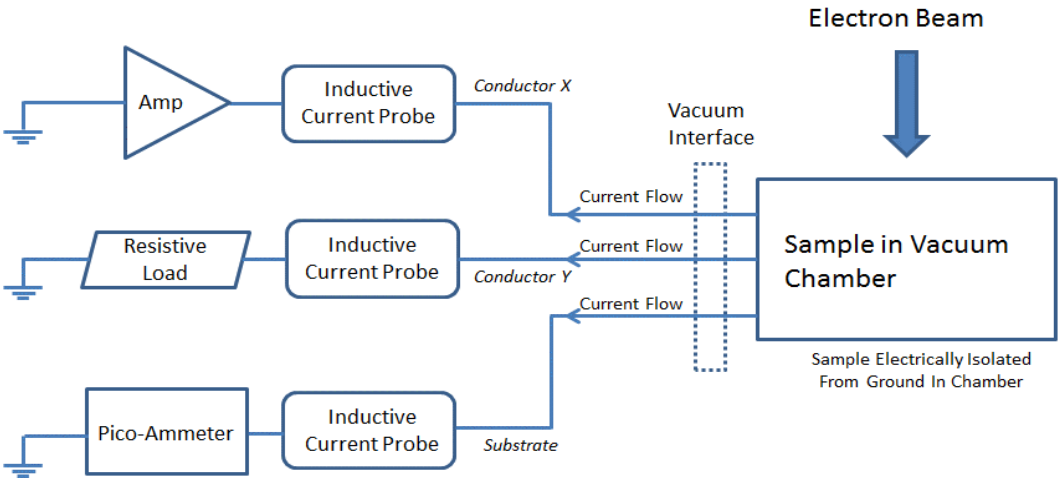

Figure 9. Block diagram of ESD detection circuitry. Common to all tests were inductive current probes. The final component before ground was changed based on sample layout and expected steady state current levels associated with collection of the primary electron beam.

To measure DC current flow, devices such as high gain current amplifiers and pico-ammeters were employed. The analog output of those devices provided a means of recording current levels throughout a given exposure by connecting the output to a data acquisition (DAQ) system. Collection of steady state currents helped confirm primary electrons were, indeed, impinging on the sample and that the electron flux from the accelerator was being maintained at constant levels. Such data was useful in situations where no ESD events, or a very limited number of ESD events, were detected. The collection of steady current in a conductor on a sample shows that an electron beam was being applied to the sample, so the lack of ESD signatures simply means that sample was not susceptible to deep charging ESD – at least for the electron beam energies and fluxes applied in that test.

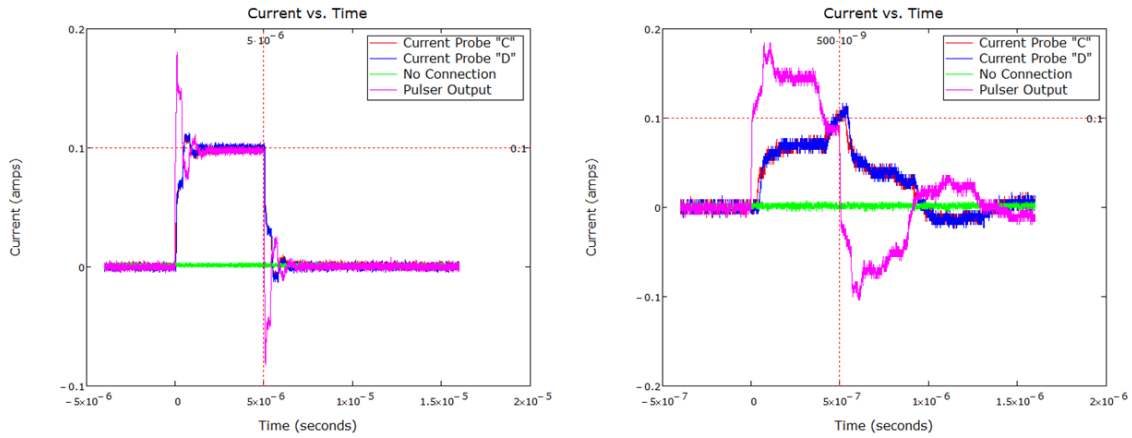

Figure 10. Data from the calibration of inductive current probes. The plot on the left shows response to a 0.1 Amp, 5 micro-second square wave test pulse (from a pulser). The right-hand plot shows the probe's response to a 500 nano-second pulse. Below ~2 micro-seconds inductive effects begin to distort the primary current pulse from the pulser, causing it to overshoot the 0.1 Amp setting.

4.4 Sample Mounting

In order to measure current pulses on samples with electrically conductive substrates, the sample had to be electrically isolated from the grounded metal sample holder so that a wire connection could be brought outside the chamber and monitored by a current probe. Isolation from ground inside the chamber was accomplished by using a Teflon standoff in each corner of the sample. The standoff was always placed behind the sample to reduce direct electron exposure. A non-conductive cable tie was used to pull the sample against the standoff and secure it to the metal sample holder plate.

5. DEEP CHARGING TESTS

Two different tests were carried out during the course of the investigation. One set of tests employed a passive circuit arrangement, while the other set of tests used an active (powered) circuit arrangement. Passive circuit tests sought to simply determine if deep charging did lead to any ESD events occurring on the sample coupon. The active circuit tests studied the impact of an ESD event on the operation of the powered systems on a coupon. In other words, would an ESD event on a powered coupon lead to damage due to generation of long duration arcs or wire-to-wire short circuit conditions?

5.1 Passive Circuit Tests

Fig. 11 is a schematic of the circuit setup for passive testing of a wire coupon. Each set of wires on the coupon along with the substrate is connected outside of the vacuum chamber to a current probe, an ammeter/amplifier, and then ground. It is important to ground the conductors on the coupon, as the deep charging electric field of interest is setup between inner charged layers of the dielectrics and the grounded conductors. Each current probe is connected to a fast oscilloscope channel. The circuit shown in Fig. 11 was effectively applied to all of the wire coupons (Front Side, Back Side, and Ribbon Harness).

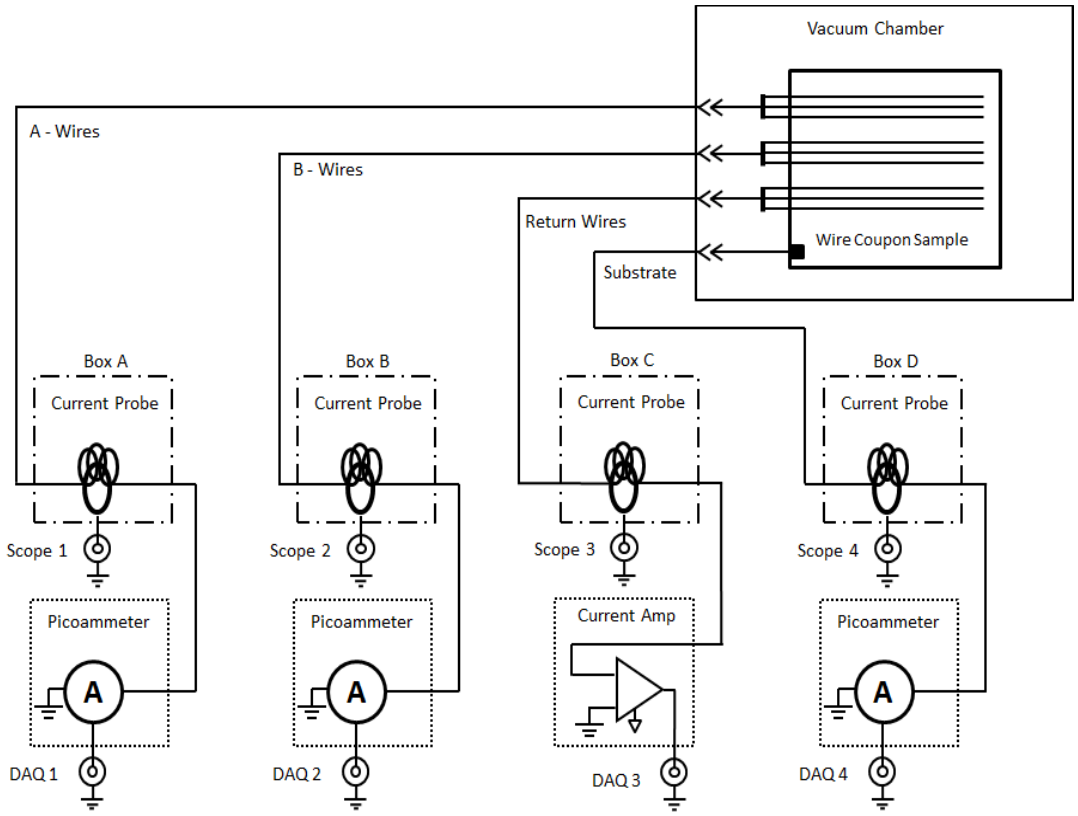

Figure 11. Wire coupon test circuit. To increase the current sensitivity, the signal wire was wrapped around the inductive current probe creating multiple turns through the probe.

The coaxial cable sample was also tested in a passive configuration. However, the external circuit arrangement differed slightly from the wire coupons setup. Fig. 12 shows the circuit schematic. Inside the vacuum chamber, the outer shield of the sample was in contact with the grounded mounting plate. A vacuum-rated flexible SMA cable connected the sample to the outside circuitry – preserving the coaxial configuration. Like the wire coupons, a current probe was connected to the inner conductor of the coaxial cable, but the system was terminated with a common circuit element used in microwave systems known as a DC Block. As the name implies, the DC Block allows microwave frequency signals to pass through it while blocking (via capacitor) DC signals, such as power signals. The DC Block circuit does, however, also include bleed resistors which are connected to ground. Therefore, the inner conductor is ultimately grounded via these resistors.

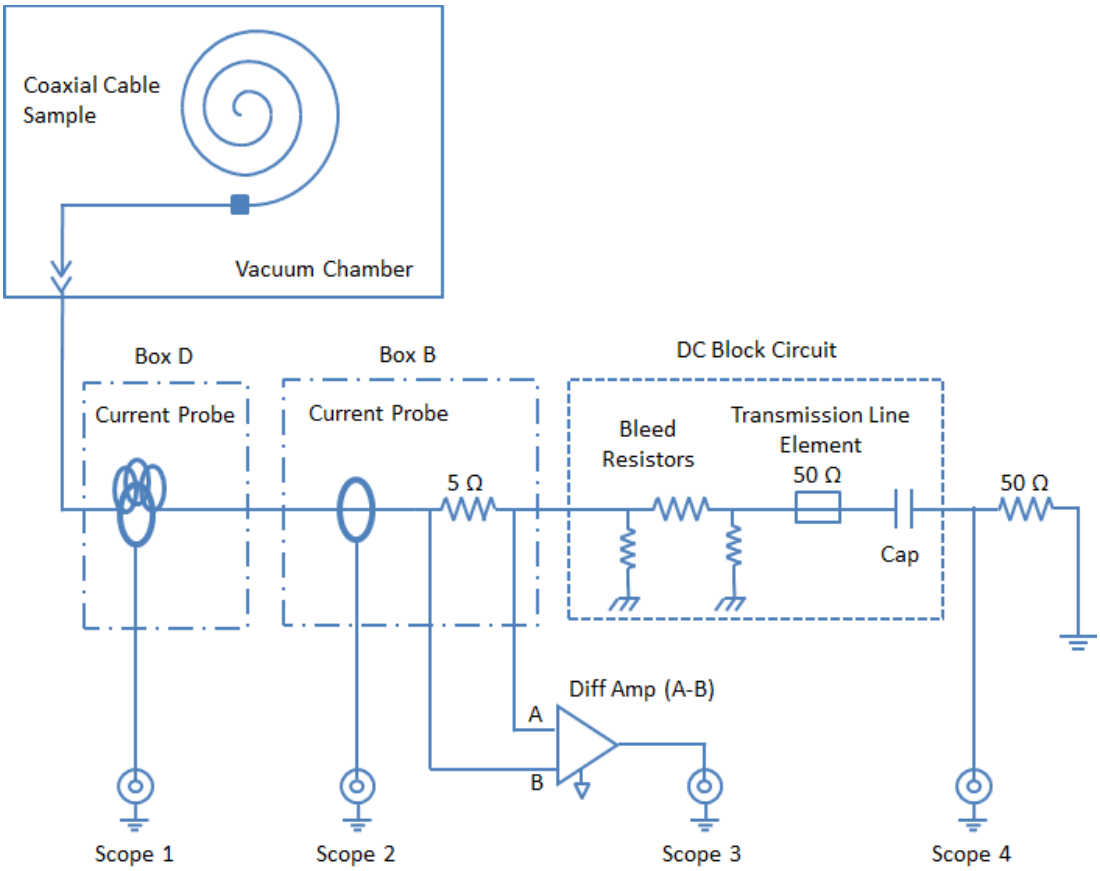

Figure 12. Coaxial cable sample test circuit with DC Block element attached.

5.2 Active (Powered) Circuit Tests

In the active circuit tests power was applied to the systems on the sample using current and voltage levels that are typical of an operational system on a satellite. The focus of these tests was to determine if deep charging ESD events could lead to damaging sustained arcs. To supply power to the coupons, a Solar Array Simulator (SAS) power supply was used. A SAS power supply is built such that it can respond to load changes very fast – in much the same way a spacecraft solar array power system would respond. It is common for SAS supplies to adjust their current output within 1 – 3 micro-seconds of a change in the load. Both the CIC coupon and the wire coupons underwent powered circuit testing. Due to space limitations, only the CIC circuit will be discussed in this paper, however the wire coupon circuit arrangement described by Wong [16] was the same as that used in the this deep charging investigation.

On the CIC coupon, the principal deep charging concern was internal charging of the coverglass on top of the photovoltaic cells and internal charging of the Kapton sheet immediately below the cells. The powered circuit test of the CIC coupon sought to determine if an arc generated by a deep discharge near the cell could lead to a secondary (sustained) arc between strings. As noted in the test article description, the CIC coupon was arranged with two parallel strings of cells. The SAS power supply was connected to the CIC coupon to apply a potential difference between the two strings. Fig. 13 shows the circuit schematic for the CIC coupon actively powered tests. This circuit was originally designed for surface charging ESD tests [17]. The circuit in Fig. 13 provides a good simulation of two strings generating power as would be the case in-flight. There is current flow through each cell as well as a

voltage between the strings and additional capacitance representing the missing cells in a complete solar array wing.

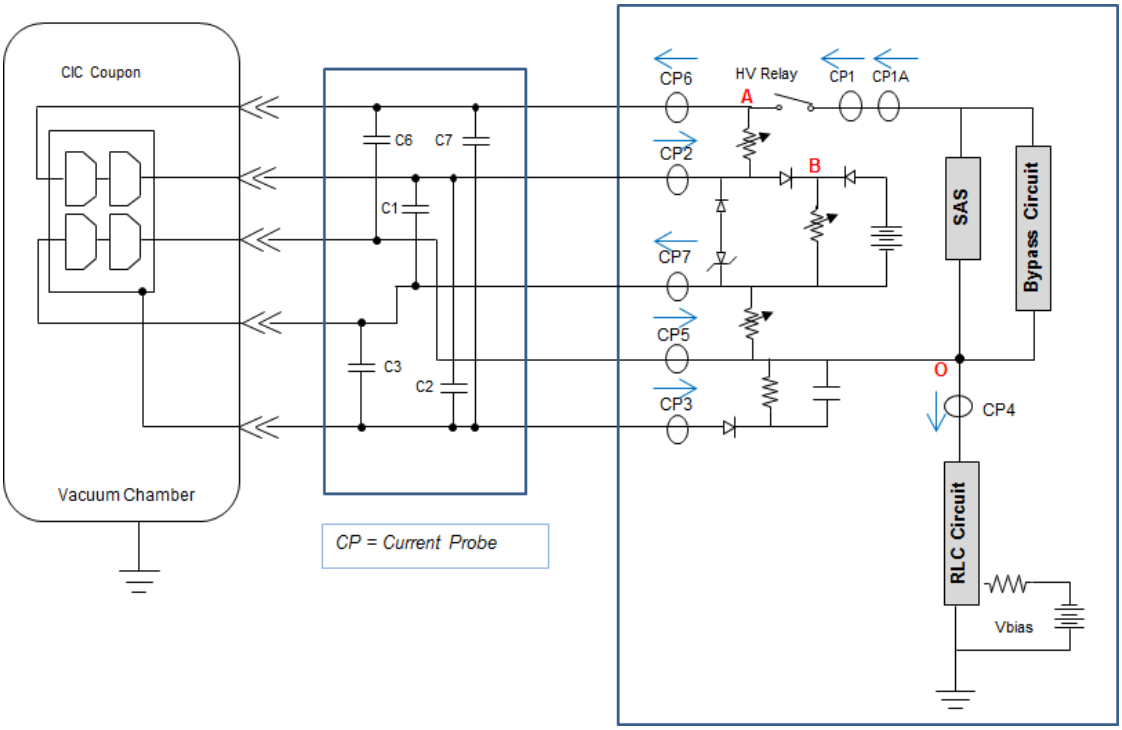

Figure 13. CIC coupon test circuit. The solar array simulator (SAS) power supply creates a potential difference between the strings on the coupon.

6. TEST RESULTS

For passive circuit testing, the task of evaluating test results centered on quantifying the number and size of ESD events generated as a result of deep charging. Theoretically, this task appears to be straightforward; unfortunately, in practice it can be quite complicated. The nature of deep charging ESD events tends to be short-duration, low-current discharges. Such discharges are capable of inducing small currents on nearby conductors. With the diagnostic setup dependent on inductive pickup current probes, the inevitable problem emerges of determining whether a signal represents a direct measurement of a deep charging ESD, or an induced signal created by a nearby ESD event. In fact, even a surface charging ESD can induce signals on the current probes and potentially be mistaken as a deep charging ESD.

To determine what constituted a true deep charging ESD event required: 1) Comparing many different recorded events and looking for distinguishing pulse shapes; and 2) Defining a minimum current magnitude threshold. Fig. 14 is an example of an event that triggered the oscilloscope to record the current probes connected to wires on the Front Side Wire coupon. All four current probe waveforms are very similar and are low in peak magnitude. Fig. 15 is another set of current probe traces from the same Front Side Wire coupon exposure as Fig. 14. Notice how channel 3 (Return-wires) has a high peak magnitude current and its waveform shape is different than channels 1, 2 and 4.

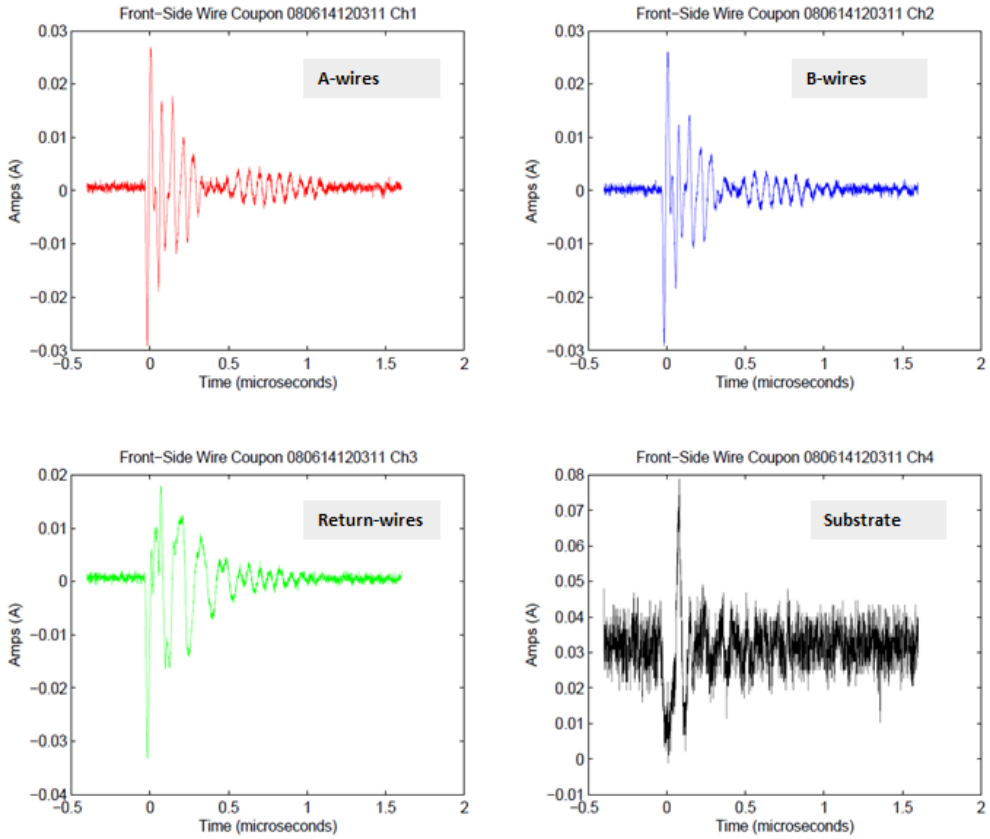

Figure 14. Recorded current probe data. Not an ESD event. All signal magnitudes are low. No unique features in any of the channels.

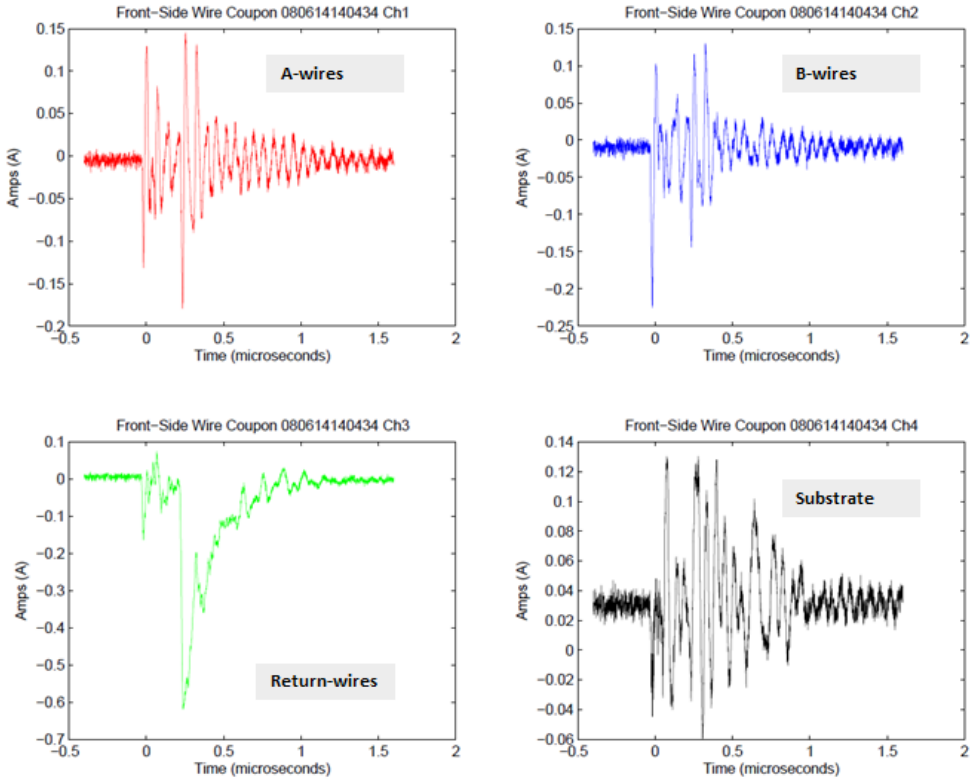

Figure 15. ESD event. Plots showing current probe data. Notice the high magnitude current signal in channel 3 which is attached to the Return-wires. The shape of the current pulse in the Return-wires is also unique compared to the other channels. The data suggest an ESD event occurred on one of the Return-wires.

After reviewing all of the recorded scope triggers for each test of the SSL test articles, and after performing a control test using a bare Aluminum plate, the test investigators established criteria for distinguishing a deep charging ESD event from a surface charging ESD event or spurious discharges somewhere in the vacuum chamber. Current probe data where all of the waveforms have the same shape, combined with low peak magnitudes, were determined to represent induced signals from a surface discharge somewhere in the chamber. Deep charging ESD events were associated with oscilloscope traces in which one waveform had a peak current many times larger than the other signals, and had a distinguishing shape (like the situation shown in Fig. 15). Applying these criteria to each passive circuit test yielded the results shown in table 3.

Table 3. Passive circuit test results summary

Passive Circuit Testing					
Sample	Electron Energy (MeV)	Exposure Time (Hours)	No. of Scope Triggers	No. of Deep Charging ESD Events	Largest Peak ESD Current Detected
Front Side Wire	0.3	5.3	65	8	700 mA
Back Side Wire	0.3	5.3	26	1	500 mA
Ribbon Harness	0.3	5.3	5	2	120 mA
Coaxial Cable (w/bleed resistors) 1.6X Flux	0.3	1.0	0	0	0 A
Coaxial Cable (w/bleed resistors) 1X Flux	1.0	1.3	0	0	0 A
Bare Aluminum (Control) 1X Flux	0.3	2.0	7	0	<200 mA
Bare Aluminum (Control) 3X Flux	0.3	0.5	6	0	<200 mA
Bare Aluminum (Control) 1X Flux	1.0	1.0	1	0	<200 mA
Bare Aluminum (Control) 8X Flux	1.0	0.5	0	0	0 A

For active (powered) circuit testing, the evaluation criteria were limited to determining whether or not deep charging led to a secondary (sustained) arc. Data from these tests was straight forward to analyze, as the signatures associated with a secondary arc are specific and well defined. In the case of a secondary arc, the SAS power supply will begin feeding current into the arc. This will extend the primary arc discharge time. Therefore, by studying the current output of the SAS one can establish whether or not a secondary (sustained) arc has occurred. The results of active circuit testing are shown in table 4.

Table 4. Active circuit test results summary

Active Circuit Testing						
Sample	Electron Energy (MeV)	Exposure Time (Hours)	SAS Voltage (Volts)	SAS Current (Amps)	No. of Scope Triggers	No. of Sustained Arc Events
CIC (Solar Cells) [1400 Volt Bias]	0.3	5.3	108	0.55	1	0
CIC (Solar Cells) [1400 Volt Bias]	1.0	1.25	108	0.55	0	0
CIC (Solar Cells) [0 Volt Bias]	0.3	5.3	108	0.55	59	0
CIC (Solar Cells) [0 Volt Bias]	1.0	1.25	108	0.55	9	0
Front Side Wire	0.3	5.3	108	4.0	11	0
Back Side Wire	0.3	5.3	108	4.0	3	0
Ribbon Harness	0.3	5.3	108	4.0	0	0

7. CONCLUSION

A set of flight-like coupons produced by Space Systems Loral has undergone a deep charging evaluation using an electron accelerator facility at NASA's Marshall Space Flight Center. The flux and fluence of electrons applied to the samples was based on levels estimated for satellites using Electric Orbit Raising, which necessitates multiple transits through Earth's radiation belts. Two electron energies were used in the evaluation (300 keV and 1 MeV). The choice of electron energies was based on calculations of the range of electrons in dielectric materials on each coupon.

The coupons were scaled versions of actual solar array systems and a communication component. The coupons were subject to passive and active (powered) configuration tests. The passive tests evaluated the size and quantity of electrostatic discharges due to deep charging. The powered tests determined if electrostatic discharges created by deep charging could lead to a secondary (sustained) arc. The nature of internal electrostatic discharges makes detecting them somewhat difficult, as they can be very fast and low in current magnitude. Also, one must separate spurious induced signals from actual electrostatic discharge events due to deep charging. Ultimately, a small number of electrostatic discharge events due to deep charging were found to occur in the passive tests. No secondary arcs were detected in the active circuit tests. Therefore, the design of the systems and components tested appears suited to withstand the high energy radiation environment associated with electric orbit raising missions.

8. REFERENCES

[1] C. A. Kluever (2004). Geostationary Orbit Transfers Using Solar Electric Propulsion with Specific Impulse Modulation. *Journal of Spacecraft and Rockets* Vol. 41, No. 3.

[2] John W. Dankanich (2010). Low-thrust Propulsion Technologies, Mission Design, and Application, *Aerospace Technologies Advancements*, Thawar T. Arif (Ed.), ISBN: 978-953-7619-96-1, InTech

[3] Craig A. Kluever, Optimal Geostationary Orbit Transfers Using Onboard Chemical–Electric Propulsion, *Journal of Spacecraft and Rockets*, Vol. 49, No. 6, November–December 2012

[4] Atri Dutta, Paola Libraro, N. Jeremy Kasdin, Edgar Choueiri, and Philippe Francken, "Minimum-Fuel Electric Orbit-Raising of Telecommunication Satellites Subject to Time and Radiation Damage Constraints", *Proceedings of the 2014 American Control Conference (ACC)*, June 4-6, 2014. Portland, Oregon, USA

[5] Horne, R. B., and D. Pitchford (2015), Space Weather Concerns for All-Electric Propulsion Satellites, *Space Weather*, 13, 430–433, doi:10.1002/2015SW001198.

[6] R. Gubby and J. Evans, Space Environment Effects and Satellite Design, *Journal of Atmospheric and Solar-Terrestrial Physics*, Volume 64, Issue 16, November 2002, Pages 1723–1733

[7] Bodeau, M. (2010), High energy electron climatology that supports deep charging risk assessment in GEO, *Proceedings of the 48th AIAA Aerospace Sciences Meeting*, Orlando, Fla., 4–7 Jan

[8] Shu T. Lai, *Fundamentals of Spacecraft Charging: Spacecraft Interactions with Space Plasmas*, Princeton University Press, 2011, ISBN 978-0-691-12947-1. pp. 246

[9] Henry B. Garrett and Albert C. Whittlesey, “Spacecraft Charging, An Update”, *IEEE Transactions On Plasma Science*, VOL. 28, NO. 6, December 2000

[10] Baker, D. N., et al., Deep dielectric charging effects due to high energy electrons in Earth's outer magnetosphere, *Journal of Electrostatics*, Volume 20, Issue 1, pp. 3-19, 1987.

[11] K.L. Bedingfield, R.D. Leach, and M.B. Alexander, Editor, Spacecraft System Failures and Anomalies Attributed to the Natural Space Environment, *NASA Reference Publication 1390*, August 1996

[12] Brian P. Beecken, Development and Application of NUMIT for Realistic Modeling of Deep-Dielectric Spacecraft Charging in the Space Environment, *Air Force Research Laboratory Report No. AFRL-RV-PS-TR-2014-0181*, 21 April 2014

[13] C. L. Lemon, J. L. Roeder, M. D. Looper, J. F. Fennell, M. J. Meshishnek, and M. R. Ciofalo, A 3-D Model of the Internal Charging of Spacecraft Dielectric Materials, *Aerospace Corporation Independent Research and Development Report*, 2010

[14] Joseph I. Minow, Modeling Electrostatic Fields Generated by Internal Charging of Materials in Space Radiation Environments, *Proceedings of the 27th International Review of Progress in Applied Computational Electromagnetics*, Applied Computational Electromagnetics Society (ACES), March 27 - 31, 2011, Williamsburg, Virginia, USA

[15] Kit Frankie Wong and Wousik Kim, Deep Charging Requirement and Analysis Approach for EOR to GEO, Paper No. 0030, *Proceedings of the 14th Spacecraft Charging Technology Conference*, ESA/ESTEC, Noordwijk, NL, 04-08 April 2016

[16] F. K. Wong et al., Electrostatic discharge tests on solar array wire coupons subjected to simulated space environment aging, *IEEE Transactions on Plasma Science*, vol. 41, no. 12, pp. 3359–3369, Dec. 2013.

[17] K. H. Wright, Jr., et al., Electrostatic discharge testing of multijunction solar array coupons after combined space environmental exposures, *IEEE Transactions on Plasma Science*, vol. 40, no. 2, pp. 334–344, Feb. 2012.